Journal of *Marine Science and Engineering*

MDPI

Article

AUV Online Path Planning Strategy Based on Sectorial Gridded Detection Area

Yang Liu [1,2,3], Jinxi Sun [3], Guojie Li [3] and Xiujun Xu [1,3,*]

[1] College of Intelligent Systems Science and Engineering, Harbin Engineering University, Harbin 150001, China; y_liu@hrbeu.edu.cn
[2] National Key Laboratory of Autonomous Marine Vehicle Technology, Harbin Engineering University, Harbin 150001, China
[3] Qingdao Innovation and Development Base, Harbin Engineering University, Qingdao 266000, China; sunjinxi@hrbeu.edu.cn (J.S.); liguojie@hrbeu.edu.cn (G.L.)
* Correspondence: xuxiujun@hrbeu.edu.cn

Abstract: In this study, an online path planning strategy capable of traversing narrow passages is proposed for an autonomous underwater vehicle equipped only with forward-looking sonar in unknown environments. First, to establish the environment model, the sonar fan-shaped detection area is subdivided into multiple sectorial grids. Then, a comprehensive cost function combining safety, smoothness, and cost is utilized to generate the optimal heading. Furthermore, to safely pass through narrow passages, a sequence of subgoals for polynomial trajectory planning are determined on the perpendicular bisector ahead of the central line. The simulation results demonstrate the effectiveness of the proposed strategy, which determines the optimal heading through fan-shaped grid costs and generates a safe and smooth path. The AUV can achieve more safety navigating in obstructed areas and narrow passages.

Keywords: autonomous underwater vehicle; path planning; sectorial gridded detection area; narrow passage traversing strategy

Academic Editor: Sergei Chernyi

Received: 19 January 2025
Revised: 13 February 2025
Accepted: 24 February 2025
Published: 26 February 2025

Citation: Liu, Y.; Sun, J.; Li, G.; Xu, X. AUV Online Path Planning Strategy Based on Sectorial Gridded Detection Area. *J. Mar. Sci. Eng.* **2025**, *13*, 443. https://doi.org/10.3390/jmse13030443

1. Introduction

The autonomous underwater vehicle (AUV) is the main platform for underwater operations [1], which has strong flexibility, concealment, adaptability, and other characteristics. By carrying various sensors and equipment, it can perform a series of tasks, such as ocean monitoring [2,3], seabed survey [4,5], resource exploration [6], and maritime search operations [7]. Path planning is an important manifestation of an AUV's autonomous capability [8], which refers to the ability to interact with the external environment. An important aspect of this interaction is the capability for global path planning, dynamic replanning in emergencies, and obstacle avoidance capabilities. Due to the complexity of the marine environment [9,10] and the weak connectivity of underwater equipment [11], limited data transmission capacity, finite energy reserves, and incomplete sensing technology for underwater operations [12] have become the main constraints in current path planning. Considering the uncertainty of the underwater environment, which is nearly impossible to predict, online path planning technology has become one of the core issues in the field of AUV research [13].

Since the 1970s, scholars from various countries have proposed multiple path planning algorithms, which comply with the following steps [14]:

- Environment modeling, that is, abstract the problems of the real world and set up corresponding models;
- Underwater positioning to obtain the position information of an AUV;
- Feasible path generating based on path planning algorithms.

According to the mastery of environmental information, path planning can be divided into global path planning for known and static obstacles and local path planning for unknown or dynamic obstacles [15–17]. Global path planning requires complete environmental information to find a path that meets the conditions through path search algorithms. On the contrary, local path planning can be performed in real-time according to the current sonar detection information. Traditional path planning methods include the A* algorithm [18], D* algorithm [19], artificial potential field method [20], etc. However, as the complexity of tasks increases, a single path planning algorithm is no longer able to adapt to complex environments and task demands [21,22]. In addition, some traditional path planning algorithms rely on known maps, which results in a separation of perception and decision-making, making it difficult to be applied in the unpredictable underwater environment. Many scholars have made improvements to traditional path planning algorithms in order to adapt to the complex marine environments. Aiming at the planning difficulties caused by the complex underwater environment and irregular obstacles, Nie proposed a dimension-reduction path planning method suitable for three-dimensional space path planning to simplify the environmental model and combined it with an improved RRT algorithm to plan the path and shorten the total distance [23]. Zhang proposed a path planning algorithm based on A* + APF to address the issue of significant path-tracking errors arising from the separate research of traditional path planning and path-tracking techniques. The proposed algorithm achieves accurate and safe path planning in complex environments with multiple obstacles but cannot guarantee the optimality of the path and practicability in large-scale unknown environments [24]. By considering the kinematic constraints and dynamic constraints of an AUV, Ehsan Taheri proposed a closed-loop rapidly exploring random tree (CL-RRT) algorithm to design a feasible path from an initial position and velocity to a target position and velocity in 3D cluttered spaces in a rapid manner, overcoming the infeasibility of path planning using traditional RRT planning [25].

With the development of computer technology, machine learning technology has gradually been employed to address some of the challenges related to AUV path planning [26]. Many researchers designed intelligent optimization path planning algorithms by drawing on intelligent decision-making and optimization methods from other disciplines, such as bionics, economics, and life science, for example, the genetic algorithm [27], ant colony algorithm [28], particle swarm algorithm [29], and neural network algorithm. Behnaz Hadi proposed an adaptive motion planning and obstacle avoidance technique based on deep reinforcement learning for an AUV. Decision-making was performed with navigation measurements and required no video image in the training phase, and a reward function was designed to produce a short, safe, and directional path towards the target. The proposed system improved anti-interference against disturbances caused by ocean currents [30]. Cao proposed an algorithm combining a bio-inspired neural network and potential field to solve the safety problem and rationality problem of path planning for an AUV in a dynamic uncertain environment, overcoming either “too close” or “too far” shortcomings. The proposed approach is computationally efficient and has better adaptability compared with other algorithms [31]. Meng proposed a smooth and secure spatial path planning algorithm that integrates the improved ant colony optimization with the corrective connected spatial search strategy, which improves the success probability of safe path planning without reducing the scope of explorable free space [32]. Lin presented an online obstacle avoidance planning method for autonomous underwater vehicles based on clockwork recurrent

neural network (CW-RNN) and long short-term memory (LSTM). With the strong learning ability and generalization ability of the obstacle avoidance algorithms, it can solve the problem of obstacle avoidance for an AUV in a dynamic or even complex environment [12]. Yan proposed a new method based on the artificial potential field method and ant colony algorithm. By combining the repulsive force field in the artificial potential field method with the pheromone in the ant colony algorithm, the local minimum point problem is solved. The results showed that the improved algorithm has certain adaptability to different search environments and is more in line with the actual application environment [33]. Compared to traditional algorithms, intelligent algorithms can better adapt to complex environments but require a long pre-learning stage and high computational costs [34]. At the same time, suffering from issues such as slow processing speed [35], poor stability and real-time capability, and a tendency to get stuck in local optima [36] poses a failing application in large-scale environments.

Path planning involves a selection of the optimal path, which often poses a multi-objective optimization problem [37]. The evaluation indicators of path planning can directly impact the effectiveness of the path planned. Commonly used evaluation indicators mainly include safety, rationality, optimality, real-time performance, and adaptability [24]. In addition, complex tasks often require an AUV to perform path planning within a limited time. A reasonable environmental model contributes to the efficiency of online path planning [38]. For the limited sonar opening angle, the vehicle can only obtain environment information within a certain angle range. The information obtained by forward-looking sonar is local information in a polar coordinate system, while the information in a grid map is based on a Cartesian coordinate system. Establishing a grid map requires coordinate system conversion, which inevitably leads to time consumption for the AUV that requires real-time collision avoidance. Moreover, when the obstacle exceeds the sensing range of the sensors, the AUV is prone to get trapped as it is not capable of detecting whether the passage between obstacles is feasible [39,40]. In addition, the vehicle entails a certain forward speed to maintain fixed-depth voyage, so most AUVs cannot maintain a stationary state to wait for path planning. Therefore, this article aims to design an efficient algorithm that enables AUVs to perform path planning in real-time at a certain speed. At the same time, narrow channels should be observed in advance so that the AUV can avoid getting stuck in concave traps.

The main contributions of this article can be summarized as follows:

- By dividing the fan-shaped sonar detection area into sectorial grids, the simplified environmental model is established, which is in line with the actual detection characteristics of sonar.
- Positioning a series of subgoals in the perpendicular bisector of the access between obstacles, which overcome the defect of the AUV's detection—disability of rear scene between obstacles at the gap, improved security of AUVs along the trajectory.
- A comprehensive cost function is utilized, integrating safety, smoothness, and distance, to achieve a multi-objective optimum so as to enhance the adaptability of the algorithm.

The remainder of this article is organized as follows: a fan-shaped, gridded environmental model is explained in Section 2; the design of the cost functions based on multiple objectives and the process of the online path planning strategy under the sectorial gridded detection area are presented in Section 3; the selection of a sequence of subgoals for steering the AUV to thread through obstacles together with the cost function of the traversing path is proposed in Section 4; the effectiveness of the proposed strategies in planning a feasible path is validated in Section 5; and finally, the article is concluded in Section 6.

2. Description and Analysis of the Problem

2.1. Establishment of Coordinate System and AUV Model

When constructing the kinematic model, it is necessary to define the positional relationship between the geodetic coordinate system and the carrier coordinate system. As shown in Figure 1, the position information of the AUV is described in the geodetic coordinate system, and the velocity information of the AUV is described in the carrier coordinate system. The axes of the earth fixed coordinate system represent the north, east, and depth directions. The axes of the carrier coordinate system represent the front, right, and bottom directions.

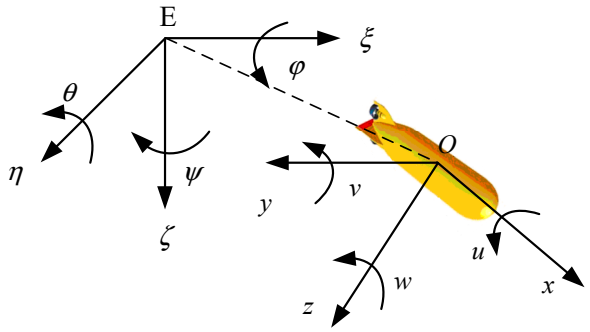

Figure 1. Geodetic coordinate system and carrier coordinate system.

This article aims to propose an effective online path planning strategy. It is assumed that the AUV navigates in fixed depth, that is, the AUV only moves in the x and y directions and rotates around the z direction. Then, the six-degree-of-freedom kinematic model in three-dimensional space is simplified to a three-degree-of-freedom kinematic model in the two-dimensional plane.

The transformation relationship in the two coordinate systems can be expressed as follows:

$$\dot{\eta} = J_{\Theta}(\eta) \cdot v \frac{1}{n} \tag{1}$$

where $\eta = [x, y, \psi]^T$ are positions and Euler angle, $v = [u, v, r]^T$ are velocity vectors, and $J_{\Theta}(\eta) \in \mathrm{R}^{3\times3}$ is the rotation transformation matrix transformed from the carrier coordinate system to the geodetic coordinate system, specifically as follows:

$$J_{\Theta}(\eta) = \begin{bmatrix} \cos\psi & -\sin\psi & 0 \\ \sin\psi & \cos\psi & 0 \\ 0 & 0 & 1 \end{bmatrix} \tag{2}$$

2.2. Mathematical Model of Sonar Vision Field

Due to the limitation of the underwater environment, acoustic sensors are the primary detection devices. A multi-beam, forward-looking sonar is employed to detect the surrounding environmental information. The forward-looking sonar is an active sonar, which can realize the detection and distance measurement of obstacles by actively emitting acoustic signals and using transducers to receive the reflected echoes. It is reasonable to assume that the obstacles are on the same horizontal plane as the AUV. The forward-looking sonar is horizontally mounted in the front of the AUV so that the sonar axis coincides with the x-axis direction of the AUV. It has a horizontal detection scope of α_H, a direction resolution for transmitted sound wave of α_R, and a detection range of R_S.

The sonar detection information can be expressed as $[d_{\text{obs}}, \alpha_{\text{obs}}]^{\mathrm{T}}$, where d_{obs} and α_{obs}, respectively, represent the distance and orientation angle of the obstacle measured

in the carrier coordinate system. Therefore, the coordinates of the obstacle in the carrier coordinate system can be expressed as follows:

$$[x_{\text{obs}}, y_{\text{obs}}]^{\text{T}} = d_{\text{obs}} \cdot [\cos\alpha_{\text{obs}}, \sin\alpha_{\text{obs}}]^{\text{T}} \tag{3}$$

As shown in Figure 2, the information of obstacle A measured by the AUV is $[d_{\text{obs}}, \alpha_{\text{obs}}]^{\text{T}}$. The position of the AUV in the geodetic coordinate system is $[x_{\text{O}}, y_{\text{O}}, \psi]^{\text{T}}$. Assuming that the distance between the sonar mount point and the geometric center of the AUV is r, then the coordinates of obstacle A in the geodetic coordinate system $\left[x_{\text{A}}^{\text{E}}, y_{\text{A}}^{\text{E}}\right]^{\text{T}}$ have the following transformation relationship:

$$\begin{bmatrix} x_{\text{A}}^{\text{E}} \\ y_{\text{A}}^{\text{E}} \end{bmatrix} = d_{\text{obs}} \begin{bmatrix} \cos\psi & -\sin\psi \\ \sin\psi & \cos\psi \end{bmatrix} \begin{bmatrix} \cos\alpha_{\text{obs}} \\ \sin\alpha_{\text{obs}} \end{bmatrix} + \begin{bmatrix} x_{\text{O}} \\ y_{\text{O}} \end{bmatrix} + r \begin{bmatrix} \cos\psi \\ \sin\psi \end{bmatrix} \tag{4}$$

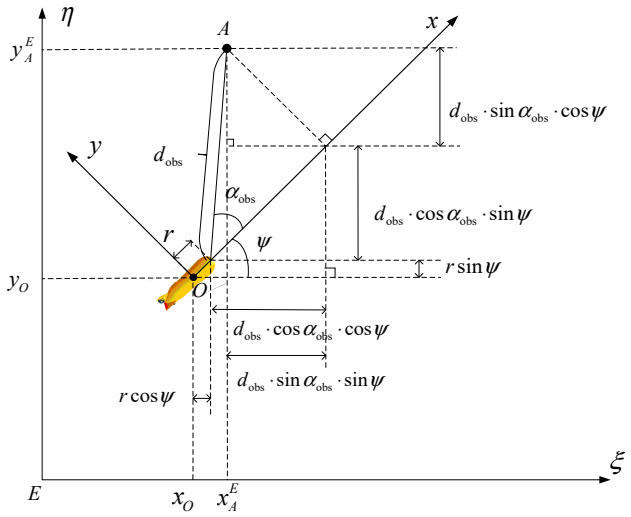

Figure 2. The conversion relationship of obstacle coordinates in two coordinate systems.

Since the sonar detection range is much longer than the length of the vehicle in practice, the latter can be ignored, and the simplified coordinates can be obtained:

$$\begin{bmatrix} x_{\text{A}}^{\text{E}} \\ y_{\text{A}}^{\text{E}} \end{bmatrix} = d_{\text{obs}} \begin{bmatrix} \cos\psi & -\sin\psi \\ \sin\psi & \cos\psi \end{bmatrix} \begin{bmatrix} \cos\alpha_{\text{obs}} \\ \sin\alpha_{\text{obs}} \end{bmatrix} + \begin{bmatrix} x_{\text{O}} \\ y_{\text{O}} \end{bmatrix} \tag{5}$$

2.3. Sectorial Grid Division of Sonar

Considering the limited open angle range, sonar can only detect a fan-shaped area. The acoustic emission array of forward-looking sonar generally emits pulse signals in a forward or vertical direction (upward or downward) through a sector. The sound wave signal emitted by the forward-looking sonar collides with an obstacle and bounces back, which is captured by the sonar receiver and converted into digital signals. These digital signals are processed to display the direction, distance, contour, etc., of the obstacle. Therefore, at a certain moment, forward-looking sonar can only detect the contour of some obstacles close to the sonar on the sector. In complex environments, when there are multiple obstacles in the sonar sector detection range, the information of the obstructed part of the obstacle located behind cannot be obtained. Therefore, it is impossible to obtain complete obstacle information for its working principle. Moreover, establishing a traditional grid model in a complex environment requires a large amount of data, which can lead to slower planning speed. The information obtained by forward-looking sonar is local information in a polar

coordinate system, while the grid map information is based on a Cartesian coordinate system. Establishing a grid map requires a coordinate system conversion, which inevitably leads to time consumption for AUVs that require real-time collision avoidance. In this article, the fan-shaped detection area of sonar on the horizontal plane is divided into several sectorial grids with vertices as the center and a certain angle as the interval, according to the geometric characteristics of sonar. The center angle of each sectorial grid, namely the resolution of the sectorial grid, is denoted as α_{F}. The sectorial grids are numbered according to the right-hand screw rule, as shown in Figure 3.

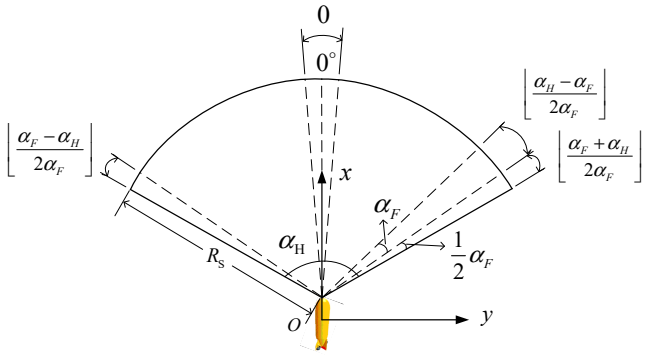

Figure 3. Schematic diagram of sectorial gridded detection area.

The sectorial grid number with a deflection angle of α can be expressed as follows:

$$i = \left\lfloor \frac{1}{\alpha_{\mathrm{F}}} \left(\alpha + \frac{1}{2}\alpha_{\mathrm{F}} \right) \right\rfloor \tag{6}$$

The deflection angle of the central axis of sectorial grid i in the carrier coordinate system can be expressed as follows:

$$\alpha_i = i \cdot \alpha_F \tag{7}$$

The detection result in the axial direction of each sectorial grid is extended to encompass the entire sectorial grid. Subsequently, a sectorial grid can be classified as either a free sectorial grid or an obstacle sectorial grid. In the case of an obstacle sectorial grid, further subdivision is executed based on the distance between the obstacle and the current position of the vehicle. If the distance is less than the minimum safety distance, it is defined as an infeasible sectorial grid; otherwise, it is defined as a far obstacle sectorial grid. Among the three aforementioned types of sectorial grids, the free sectorial grid and the far obstacle sectorial grid are considered feasible sectorial grids, and the AUV travels along the central axis direction of the sectorial grid.

3. Optimal Heading Selection Based on Sectorial Grid Model

The vehicle's heading is determined in the light of the sectorial grid cost, which is structured blending with evaluation indicators as follows:

- Security: The planned path is safe and collision-free.
- Smoothness: A smooth path can improve the efficiency of path tracking.
- Distance: The path is optimal at the specified distance measurement.

3.1. Safety Constraints

The AUV is threatened by obstacles from the relative distance and heading. For sectorial grid i, the obstacle cost function is related to two aspects: the relative distance

between the obstacle in sectorial grid i and the vehicle together with the relative deflection angle between sectorial grid i and any sectorial grid where obstacles exists.

For sectorial grid i, the threat degree of obstacle distance can be expressed as follows:

$$th^i_{dobs} = \begin{cases} 1 & , \ d^i_{obs} \in \left[\ 0 \ , \ d_{safe} \ \right) \\ 1 - 2\left(\frac{d^i_{obs} - d_{safe}}{R_S - d_{safe}}\right)^2 & , \ d^i_{obs} \in \left[d_{safe} \ , \ \frac{d_{safe}+R_S}{2} \right) \\ 2\left(\frac{R_S - d^i_{obs}}{R_S - d_{safe}}\right)^2 & , \ d^i_{obs} \in \left[\frac{d_{safe}+R_S}{2} \ , \ R_S \right) \\ 0 & , \ d^i_{obs} \in \left[\ R_S \ , \ +\infty \ \right) \end{cases} \tag{8}$$

where d^i_{obs} represents the Euclidean distance between the obstacle on sectorial grid i and the current position of AUV. If there is no obstacle in sectorial grid i, d^i_{obs} is considered to be infinite. d_{safe} represents the minimum safety distance, and R_S is the maximum detection range of sonar.

The threat degree increases as the relative distance between the obstacle and AUV decreases, and it reaches the maximum when the relative distance is under the minimum safety distance.

Based on the obstacle distance threat degree, the obstacle distance threat cost of sectorial grid i is given as follows:

$$C^i_{dobs} = \begin{cases} +\infty, & th^i_{dobs} = 1 \\ th^i_{dobs}, & \text{others} \end{cases} \tag{9}$$

The heading threat degree of obstacles on any obstacle sectorial grid j to sectorial grid i can be expressed in the form of a Gaussian function:

$$th^i_{\psi obsj} = \begin{cases} e^{-\frac{(i-j)^2}{2\sigma_{\psi obs}{}^2}}, & |i-j| \le N_{gap} \\ 0, & others \end{cases} \tag{10}$$

where i represents the number of the sectorial grid to be selected, j represents the number of the sectorial grid where the obstacle is located, N_{gap} is the maximum number of interval sectorial grids affected by the obstacle heading threat in the sectorial grid to be selected, and $\sigma_{\psi obs}$ is the obstacle heading threat degree parameter.

The sectorial grid is not threatened by the heading from the obstacle when the obstacle is far from the sectorial grid.

Sectorial grid i is threatened by the heading of obstacles from each sectorial grid j, so the cost of obstacle heading threat can be expressed as follows:

$$C^i_{\psi obs} = \frac{1}{2N_{gap}+1} \sum th^i_{\psi obsj} \tag{11}$$

3.2. Smoothness Constraint

Smooth paths can enhance the effectiveness of subsequent path tracking, thereby improving the efficiency of online path planning. To improve path smoothness and reduce sharp turns, it is necessary to constrain the turning angle of the AUV. The relative heading cost of the sectorial grid increases with the angle, and the relative heading cost of sectorial grid i can be expressed as a Gaussian-type function:

$$C^i_{\alpha F} = 1 - e^{-\frac{\alpha^i_{UUV}{}^2}{2\sigma_{\alpha F}{}^2}} \tag{12}$$

where $\sigma_{\alpha F}$ represents the angle constraint parameter, and the specific expression of α_{UUV}^{i} is shown in Equation (7), which represents the heading angle of the sectorial grid i in the carrier coordinate system.

3.3. Distance Evaluation

The planned path usually needs to be as short as possible. To reach the terminal point as soon as possible, selections tend to the sectorial grids where the heading and distance are closer. The cost of sectorial grid deviation from the ending point heading can be expressed by a Gaussian-type function:

$$C_{dev}^{i} = 1 - e^{-\frac{(\psi_{Udev}+\alpha_i)^2}{2\sigma_{dev}^2}} \tag{13}$$

where σ_{dev} represents the ending point deviation loss parameter, $\psi_{Udev} = \psi_{UUV} - \psi_{end}$ represents the angle between the heading of the AUV and the ending point direction, ψ_{UUV} represents the heading angle of the AUV in the geodetic coordinate system, and ψ_{end} represents the angle of the direction from the AUV to the ending point in the geodetic coordinate system.

In an ideal obstacle-free environment, the optimal moving direction is towards the ending point. However, in practice, the vehicle generates additional paths for obstacle avoidance.

As is illustrated in Figure 4, l_{u_e} is the Euclidean distance from the AUV to the ending point, assuming that the position and heading of the AUV at the current moment are $[x_u, y_u, \psi_u]^T$ and the vehicle performs linear motion during the planning cycle. The Euclidean distance between the AUV and the path point at the next time is l_T. Then, the node coordinates that the AUV reaches at the next time of sectorial grid i in the geodetic coordinate system can be obtained as follows:

$$P_F^i = l_T \cdot \begin{bmatrix} \cos\psi_u & -\sin\psi_u \\ \sin\psi_u & \cos\psi_u \end{bmatrix} \begin{bmatrix} \cos\alpha_i \\ \sin\alpha_i \end{bmatrix} + \begin{bmatrix} x_u \\ y_u \end{bmatrix} \tag{14}$$

where α_i represents the heading angle of sectorial grid i in the carrier coordinate system, as is shown in Equation (7).

The Euclidean distance between the path point P_F^i, the next moment, and the ending point is $l_{F\_e}^i$. When moving towards the ending point, the next path point is P_o, and the Euclidean distance from P_o to the ending point is as follows:

$$l_{o\_e} = l_{u\_e} - l_T \tag{15}$$

The additional path generated by selecting sectorial grid i is as follows:

$$\Delta l_i = l_{F\_e}^i - l_{o\_e} \tag{16}$$

When the vehicle moves towards the ending point directly, the minimum Δl_i is 0. When the vehicle moves away from the ending point in the opposite direction, the maximum Δl_i is $2l_T$.

Therefore, the following path cost function is selected:

$$C_{rextra}^{i} = \begin{cases} \frac{1}{2}\left(\frac{\Delta l_i}{l_T}\right)^2, & \Delta l_i \in [0, l_T) \\ 1 - \frac{1}{2}\left(\frac{\Delta l_i - 2l_T}{l_T}\right)^2, & \Delta l_i \in [l_T, 2l_T] \end{cases} \tag{17}$$

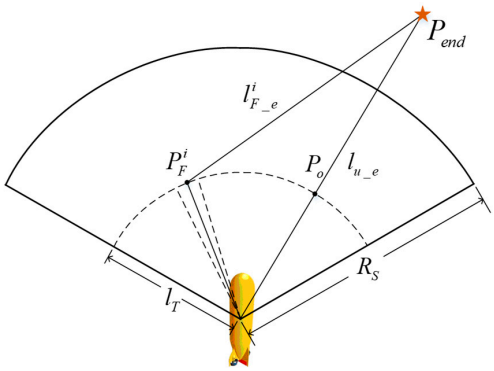

Figure 4. Additional path generated by sectorial grid obstacle avoidance.

3.4. Comprehensive Cost Function

Assigning weights to each item, the comprehensive cost function is composed through a linear weighting method:

$$C^i_a = \omega_1 \cdot C^i_{dobs} + \omega_2 \cdot C^i_{\psi obs} + \omega_3 \cdot C^i_{\alpha F} + \omega_4 \cdot C^i_{dev} + \omega_5 \cdot C^i_{rextra} \tag{18}$$

where $\omega_m (m = 1, 2, \ldots, 5)$ is the weight coefficient.

Therefore, the optimal sectorial grid for sailing is $i^* = \underset{i}{\operatorname{argmin}}\, C^i_a$.

3.5. Heading Selection Process Based on Sectorial Grid

The AUV entails detections at regular intervals for the surrounding environment and plans the path in real-time in seaway. The process of heading selection in the online path planning strategy based on a fan-shaped grid during the period T is shown in Algorithm 1.

Algorithm 1 The Process of Heading Selection Based on Fan-shaped grid

Input: Position and heading of AUV $[x_u, y_u, \psi_u]^T$, destination position $[x_e, y_e]^T$, Obstacle information $Obs = \left\{ \left(d^{obs}_m, \alpha^{obs}_m \right) \middle| m \in [1, M] \right\}$

1: Termination condition judgment.

If the ending point is arrived, end the path planning task.

2: Establish sectorial grid model.

Divide fan-shaped detection area following the rules in Section 2 and calculate the serial number of each sectorial grid according to (6).

Establish a matrix to store obstacle information on the axis of the sectorial grids.

3: Heading selection based on sectorial grid.

Calculate obstacle distance threat cost C^i_{dobs} for each sectorial grid, as expressed in (9);

Calculate obstacle heading threat cost $C^i_{\psi obs}$ for each sectorial grid, as expressed in (11);

Calculate relative heading cost $C^i_{\alpha F}$ for each sectorial grid, as expressed in (12);

Calculate termination heading deviation cost C^i_{dev} for each sectorial grid, as expressed in (13);

Calculate additional path cost for each sectorial grid, as expressed in (17);

Calculate the comprehensive cost C^i_a of each sectorial grid, as expressed in (18), and select the sectorial grid with the lowest cost to sail. Then turn to output.

Output: The optimal heading ψ_{next}

4. Narrow Passage Traversing Strategy Based on Perpendicular Bisector

When obstacles exceed the sonar detection range, the vehicle can easily fall into a concave trap. To thread through narrow passages safely, the perpendicular bisector is employed to find a set of subgoals, which can guide path planning. The polynomial

trajectory planning method is used to adjust the heading on the way to the subgoal so as to observe the environment in advance and ensure that the AUV avoids getting stuck in concave traps.

4.1. Design of Planning Strategy

The AUV distinguishes multiple obstacles detected during the voyage. When two obstacles present in sectorial grids, the clearance between the two obstacles is compared with the minimum safe passage width of the AUV. If it is sufficient for the AUV to pass safely, the narrow passage is considered to exist.

As is illustrated in Figure 5, the two nearest obstacle points between two adjacent obstacles are connected under the sectorial grid model. The perpendicular bisector is made crossing the midpoint P_{mid} of the segment between obstacles, and a point P_{sub} on the perpendicular bisector is selected as the subgoal at a distance of d_{safe} from the midpoint P_{mid}.

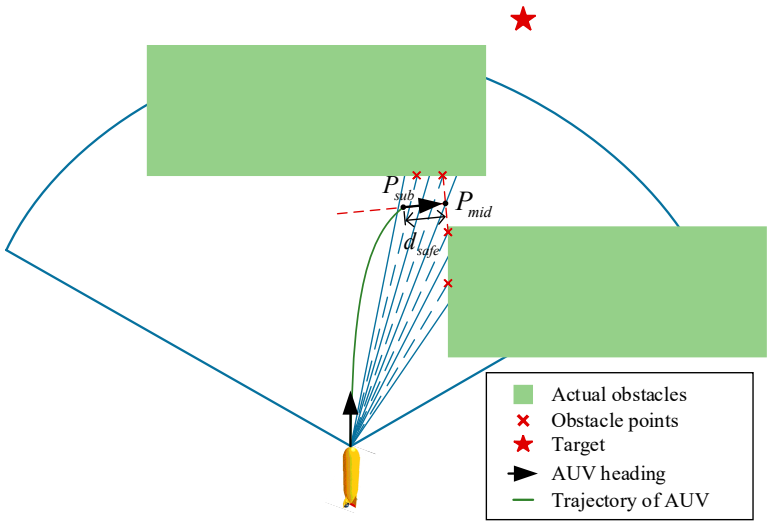

Figure 5. The path through the narrow passage based on perpendicular bisector.

The polynomial trajectory planning algorithm is employed to plan a smooth trajectory from the starting point as the current heading to the ending point as the direction from P_{sub} to point P_{mid}, with the current position of the AUV as the starting point and the subgoal P_{sub} as the ending point. When the AUV drives along a predetermined trajectory towards the subgoal, the environment is detected at certain time intervals to continuously update the position of the subgoal and update the trajectory based on the current state of the vehicle.

Based on the boundary constraints at the starting and target points, determine the third-order polynomial trajectory equation as follows:

$$\begin{cases} x(t) = a_0 + a_1 t + a_2 t^2 + a_3 t^3 \\ y(x) = b_0 + b_1 x + b_2 x^2 + b_3 x^3 \end{cases} \tag{19}$$

Combine the AUV kinematic model to solve the coefficients in the polynomial trajectory equations:

$$\begin{bmatrix} a_0 \\ a_1 \\ a_2 \\ a_3 \end{bmatrix} = \begin{bmatrix} 1 & t_0 & t_0^2 & t_0^3 \\ 0 & 1 & 2t_0 & 3t_0^2 \\ 1 & t_f & t_f^2 & t_f^3 \\ 0 & 1 & 2t_f & 3t_f^2 \end{bmatrix}^{-1} \begin{bmatrix} x_u \\ u\cos\psi_u \\ x_{sub} \\ u\cos\psi_{sub} \end{bmatrix} \tag{20}$$

$$\begin{bmatrix} b_0 \\ b_1 \\ b_2 \\ b_3 \end{bmatrix} = \begin{bmatrix} 1 & x_u & x_u^2 & x_u^3 \\ 0 & 1 & 2x_u & 3x_u^2 \\ 1 & x_{sub} & x_{sub}^2 & x_{sub}^3 \\ 0 & 1 & 2x_{sub} & 3x_{sub}^2 \end{bmatrix}^{-1} \begin{bmatrix} y_u \\ \tan\psi_u \\ y_{sub} \\ \tan\psi_{sub} \end{bmatrix} \tag{21}$$

where $\begin{bmatrix} x_u & y_u & \psi_u \end{bmatrix}^T$ represents the position and heading of the AUV at the starting point. $\begin{bmatrix} x_{sub} & y_{sub} & \psi_{sub} \end{bmatrix}^T$ represents the position and heading of the AUV at the local target point. t_0 and t_f are the corresponding moments at the starting and ending points, respectively.

Similar to the sectorial grid selection method, the traversing cost of the narrow passage also needs to be estimated. The sailing path will be determined by comparing the comprehensive cost of the two strategies. The cost of the traversing path is designed from three aspects: security, smoothness, and distance.

4.2. Design of Cost Function

4.2.1. Safety Constraints of Narrow Passage Traversing Strategy

The width of the passageway is the key problem that needs to be taken into account to ensure the safety of trajectory. The threat degree of the width of the narrow passage for the AUV to path through can be expressed as follows:

$$th_{wobs}^{sub} = \begin{cases} 1 & , w_o \in \left[0, w_{safe}\right) \\ 1 - 2\left(\frac{w_o - w_{safe}}{w_{abs} - w_{safe}}\right)^2 & , w_o \in \left[w_{safe}, \frac{w_{safe}+w_{abs}}{2}\right) \\ 2\left(\frac{w_{abs} - w_o}{w_{abs} - w_{safe}}\right)^2 & , w_o \in \left[\frac{w_{safe}+w_{abs}}{2}, w_{abs}\right) \\ 0 & , w_o \in \left[w_{abs}, +\infty\right) \end{cases} \tag{22}$$

where w_o represents the minimum width of the distance between the two obstacles detected by the AUV at the current position, w_{safe} represents the minimum width that sustains the AUV to thread, and w_{abs} represents the minimum width of absolute safety.

The safe traversing cost of narrow passage can be expressed as follows:

$$C_{wobs}^{sub} = \begin{cases} th_{wobs}^{sub}, & others \\ +\infty, & th_{wobs}^{sub} = 1 \end{cases} \tag{23}$$

In addition, the vehicle is threatened by the heading of surrounding obstacles. The heading threat of obstacles to the threading course can be expressed as the heading threat to the sectorial grid where the subgoal is located. The heading angle of the subgoal in the carrier coordinate system is α_{sub}, which is expressed as follows:

$$\alpha_{sub} = \arctan\left(\frac{y_{sub} - y_u}{x_{sub} - x_u}\right) - \psi_u \tag{24}$$

The sectorial grid number n_{sub} can be obtained from (6). The obstacle heading threat $th_{\psi obs}^{sub}$ and the corresponding cost $C_{\psi obs}^{sub}$ can be determined by Equations (10) and (11).

4.2.2. Smoothness Constraint of Narrow Passage Traversing Strategy

The path smoothness is mainly achieved by avoiding sharp turns. Therefore, the smoothness of the traversing path can be estimated by the deflection angle from the vehicle's position to the subgoal. The deviation angle of the AUV from the current heading

to the heading at the subgoal is ψ_{u_sub}, which is expressed as $\psi_{u\_sub} = \psi_{sub} - \psi_u$, and the cost of heading deviation of the traversing path can be expressed as follows:

$$C_{\Delta\psi}^{sub} = 1 - e^{-\frac{\psi_{u\_sub}^2}{2\sigma_{\alpha F}^{sub\,2}}} \tag{25}$$

where $\sigma_{\alpha F}^{sub}$ represents the angle constraint parameter of the traversing path.

4.2.3. Distance Evaluation of Narrow Passage Traversing Strategy

The distance cost of the threading course is evaluated by the departure degree of the ending point and the additional path. The angle between the line connecting the AUV to the subgoal and the line connecting the AUV to the ending point is described as the deviation angle of the traversing path, denoted by ψ_{dev}^{sub}, specifically as follows:

$$\psi_{dev}^{sub} = \arctan\left(\frac{y_{end} - y_u}{x_{end} - x_u}\right) - \arctan\left(\frac{y_{sub} - y_u}{x_{sub} - x_u}\right) \tag{26}$$

The heading deviation cost of the traversing path C_{dev}^{sub} can be determined by (13).

Since the length of the driving path is hard to measure correctly with incomplete environmental information, a roughly estimated distance is given by setting critical path nodes. As shown in Figure 6, the key path node of the threading path is the subgoal P_{sub}. l_{u_sub} and l_{sub_e} represent the Euclidean distance from the AUV to P_{sub} and from P_{sub} to the terminal point, respectively. The length of the traversing path, thereby, can be expressed as follows:

$$l_{narrow} = l_{u\_sub} + l_{sub\_e} \tag{27}$$

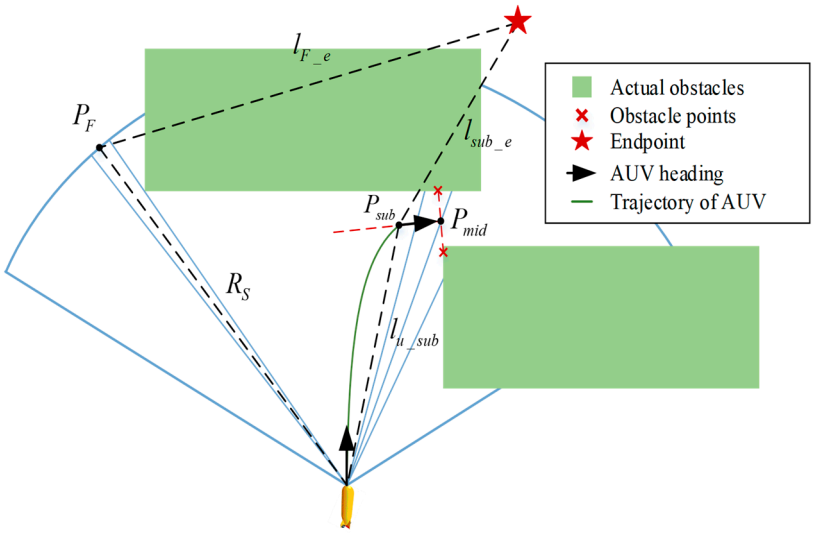

Figure 6. Additional path traversing the narrow passage.

According to the previous section, the AUV makes a detour to avoid obstacles, which causes an extra path. As shown in Figure 6, a critical path node P_F is selected on the free sectorial grid with the minimum deviation angle. The Euclidean distance from the AUV to P_F is the maximum detection range of the sonar R_S, and the Euclidean distance from P_F to the ending point is l_{F_e}. The path length for sectorial grid obstacle avoidance can be expressed as follows:

$$l_F = R_S + l_{F\_e} \tag{28}$$

Therefore, the additional path cost of traversing the narrow passage can be expressed as follows:

$$C_{rextra}^{sub} = \begin{cases} 0 & , l_{sub} \in [0, l_F) \\ 2\left(\frac{l_{sub}-l_F}{l_c-l_F}\right)^2 & , l_{sub} \in \left[l_F, \frac{l_F+l_c}{2}\right) \\ 1-2\left(\frac{l_{sub}-l_c}{l_c-l_F}\right)^2 & , l_{sub} \in \left[\frac{l_F+l_c}{2}, l_c\right) \\ 1 & , l_{sub} \in [l_c, +\infty) \end{cases} \tag{29}$$

where l_c is a constant.

4.2.4. The Comprehensive Cost of the Traversing Path

The synthesize cost for sailing between the narrow obstacles can be obtained by employing a linear weighting method:

$$C_{sub} = \omega_1^{sub} \cdot C_{wobs}^{sub} + \omega_2^{sub} \cdot C_{\psi obs}^{sub} + \omega_3^{sub} \cdot C_{\Delta\psi}^{sub} + \omega_4^{sub} \cdot C_{dev}^{sub} + \omega_5^{sub} \cdot C_{rextra}^{sub} \tag{30}$$

where $\omega_m^{sub}(m = 1, 2, \ldots, 5)$ represents the weight coefficient.

4.3. Online Path Planning Process

When a narrow passage is detected during the AUV's voyage, a measurement of its width is carried out. If the narrow passage is feasible, the subgoal would be obtained using the perpendicular bisector. Then, the cost of the traversing path is calculated and compared with the minimum sectorial grid cost. The path with the lower cost is chosen to sail. The process of AUV online path planning in a planning cycle T is illustrated in Algorithm 2.

Algorithm 2 Online path planning algorithm process

Input: Position and heading of AUV $[x_u, y_u, \psi_u]^T$, Ending point position $[x_e, y_e]^T$
1: Termination condition judgment.
If the ending point is arrived, end the path planning task.
2: Establishing the environmental model
Detect the surrounding environment and obtain obstacle information $Obs = \left\{ \left(d_m^{obs}, \alpha_m^{obs} \right) \middle| m \in [1, M] \right\}$;
Establish sectorial grid model according to obstacle information.
3: Heading selection based on sectorial grid.
Calculate the minimum sectorial grid cost C_{min}^{Fan} and the heading ψ_{Fan} of the sectorial grids.
4: Narrow passage existence judgment
If the narrow passage exists, turn to step 5. Otherwise, turn to step 6.
5: Narrow passage crossing strategy based on perpendicular bisector.
Calculate the coordinates of the subgoal P_{sub} and the heading ψ_{sub} of AUV at this location;
Calculate the cost of the narrow passage C_{sub}, as expressed in (30);
Compare the values of the minimum sectorial grid cost C_{min}^{Fan} and the narrow passage cost C_{sub}. If the former is smaller, employ the polynomial trajectory planning method to plan the local path through the narrow passage; on the contrary, plan the sectorial grid path.
Output: Path point set

5. Simulation Results and Discussion

In this paper, based on the SeaBat F50 (Teledyne RESON, Slangerup, Denmark) high-resolution, forward-looking, multi-beam Sonar, a model of the environment in the scope of sonar is established. The specific parameters are shown in Table 1. To facilitate the research, the sectorial grid resolution is set to 2°; thus, the sonar detection area can be divided into 65 small sectorial grids. The cruising speed of the AUV is 2 m/s. The planning cycle is 50 s. Other parameter settings in the simulation are shown in Table 2.

Table 1. Parameters of the multi-beam, forward-looking sonar.

Parameters	Values
Horizontal detection scope α_{H}	128°
Number of horizontal beams M	256
Max update rate f_{up}	50 Hz
Direction resolution α_{R}	1°
Range R_{S} (up to)	500 m

Table 2. Parameters in the algorithm.

Parameters	Values	Parameters	Values
d_{safe}	150 m	w_{safe}	20 m
$\sigma_{\psi obs}$	3	w_{abs}	40 m
N_{gap}	4	$\sigma_{\alpha F}^{sub}$	25
$\sigma_{\alpha F}$	33	σ_{dev}	60
ω_1	0.244	ω_1^{sub}	0.133
ω_2	0.146	ω_2^{sub}	0.133
ω_3	0.220	ω_3^{sub}	0.267
ω_4	0.244	ω_4^{sub}	0.200
ω_5	0.146	ω_5^{sub}	0.267

5.1. Simple Obstacle Environment Simulation

The coordinates of the starting point and ending point of path planning in the geodetic coordinate system are $(100, 100)$ and $(600, 1000)$, respectively. Two polygons are set as obstacles, and the parameters are shown in Table 3.

Table 3. Conventional obstacle parameters.

Number	Number of Sides/m	Vertex Coordinates/m
1	4	(150, 200), (150, 450), (300, 450), (300, 200)
2	3	(450, 550), (300, 800), (450, 800)

The simulation results are shown in Figure 7. The AUV obtains obstacle information from the multi-beam, forward-looking sonar, and the sonar data during sailing are plotted on the map. Obviously, the AUV can plan a safe and collision-free smooth path.

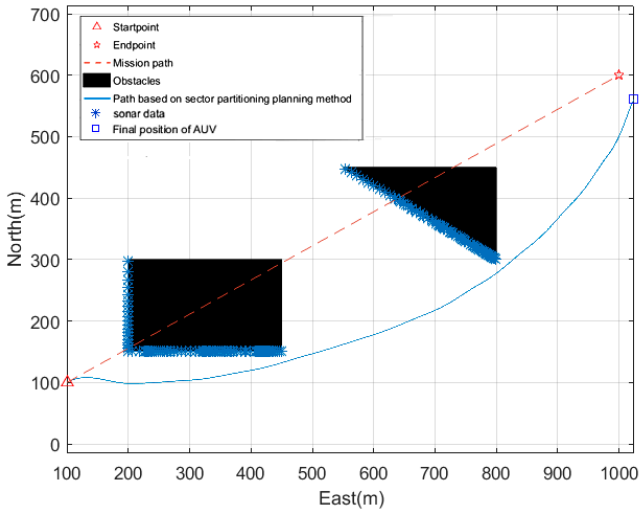

Figure 7. Avoidance result in simple obstacle environments.

5.2. Narrow Passage Traversing Simulation

To verify the effectiveness of the algorithm, two polygonal obstacles with extremely close clearance were installed, which forms a narrow passage. Multiple comparative simulation experiments were conducted by setting different narrow passage widths. In the simulation, the minimum safe transit width of the narrow passage w_{safe} is 20 m.

The coordinates of the starting point and the ending point in the geodetic coordinate system are $(500, 500)$ and $(1100, 1200)$, respectively. The minimum spacing between the two obstacles is 35 m, and the obstacle parameters are shown in Table 4.

Table 4. Obstacle parameters with narrow passage.

Number	Number of Sides/m	Vertex Coordinates/m
1	4	(935, 700), (935, 1050), (1300, 1050), (1300, 700)
2	3	(900, 1000), (500, 1200), (900, 1300)

The simulation results are illustrated in Figures 8–11.

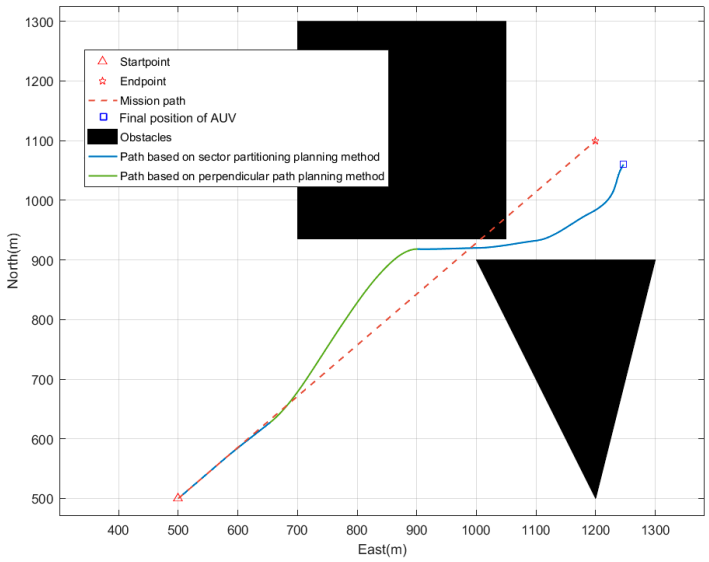

Figure 8. Result of traversing the narrow passage.

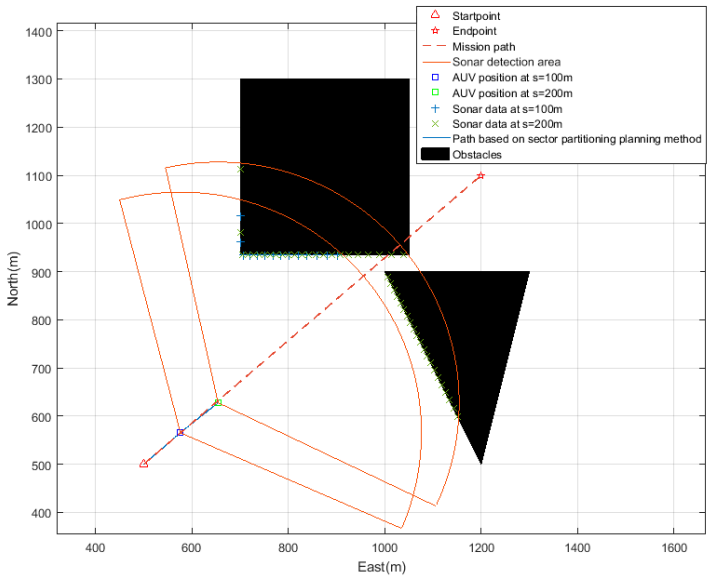

Figure 9. Obstacle avoidance scene at s = 100 m and s = 200 m.

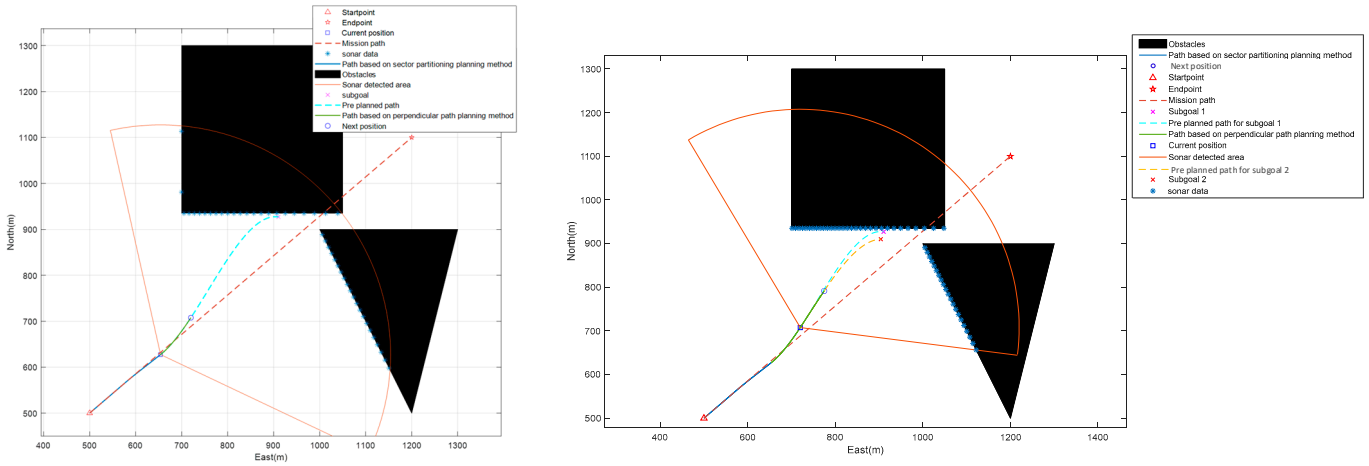

(**a**) (**b**)

Figure 10. Path planning for traversing the narrow passage. (**a**) Start using narrow passage traversing strategy. (**b**) The sub targets are constantly adjusted as the AUV navigates.

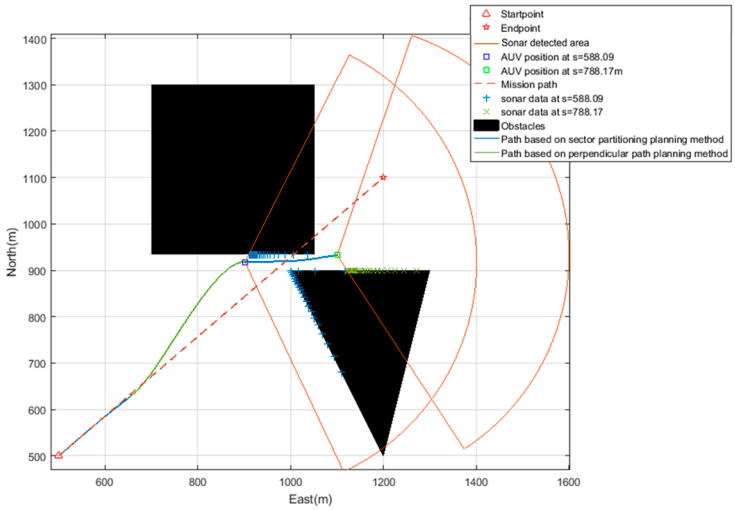

Figure 11. Obstacle avoidance scene at s = 588.09 m and s = 788.17 m.

Figure 8 shows the complete path, indicating that the AUV plans a safe and smooth threading course, with a total length of 993 m.

In Figure 9, the AUV is located at the path length s = 100 m, and the obstacles are relatively far from the AUV at the beginning of the voyage. Due to the inability to detect obstacles in the direction of the ending point, the AUV sailed towards the ending point. The obstacles were displayed on continuous sectorial grids at the path length s = 200 m along with the approaching AUV. Since the vehicle failed to see the exit of the narrow passage for its heading angle, the perpendicular bisector was employed to determine the subgoal and plan a safe traversing path in the condition of a feasible passage width.

The process of starting to execute the narrow passage traversing strategy is shown in Figure 10. As the AUV drove to the narrow passage, the subgoal was adjusted accordingly. The heading of the AUV was ultimately towards the exit of the narrow passage.

The vehicle traversed safely and traveled in the middle of the narrow passage as much as possible by applying the sectorial grid path planning method, as is shown in Figure 11.

To demonstrate the effectiveness of the algorithm, a set of comparative simulation experiments were conducted. When the perpendicular path planning method is not implemented, the path planned by the AUV and the selection of the sectorial grids are shown in Figure 12. By comparing with previous simulation experiments, it can be seen

that, although the AUV successfully passes through the narrow passage using the online path planning method, the planned path is too close to the obstacles, which may pose a danger during actual sailing.

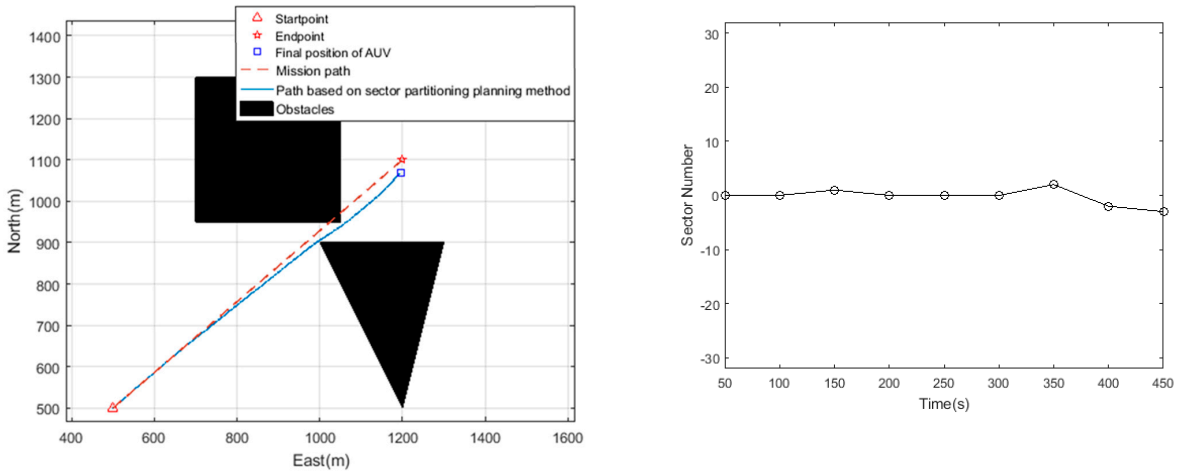

(**a**) (**b**)

Figure 12. The results of traversing the narrow passage without subgoals and the selection of fan-shaped grids. (**a**) Traversing the narrow passage without subgoals. (**b**) Sectorial grid selection of the AUV.

For the elongated narrow passage in the environment, as shown in Figure 8, the perpendicular path planning method is used for safe traversing, and the planned path can be kept in the middle of the passage.

When the narrow passage is blocked at the end, the path planned using the proposed perpendicular path planning method is shown in Figure 13a. During the initial sailing process, the AUV was unable to see the scene at the end of the passage. By using the proposed perpendicular path planning method, the AUV can obtain the knowledge of indentations and decide whether they can be safe accesses once it reaches the vicinity of the subgoal. Due to the minimum safe distance between the subgoal and the entrance of the passage, the AUV can turn and find other feasible paths in a timely and safe manner.

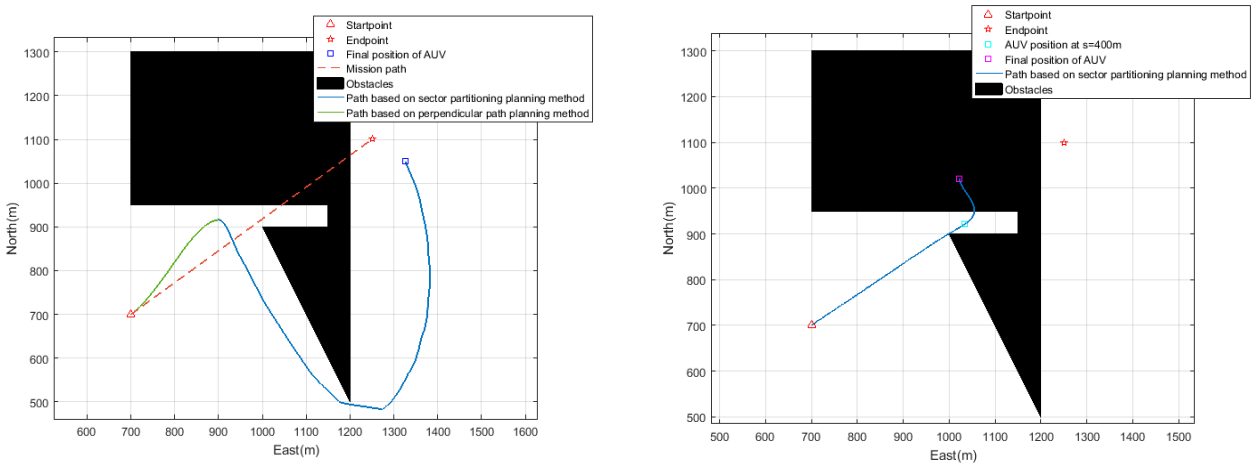

(**a**) (**b**)

Figure 13. Comparing the results of path planning using and not using the perpendicular path planning method when the end of the narrow passage is impassable. (**a**) Result of using the perpendicular path planning method. (**b**) Result without subgoals.

Figure 13b shows the comparative results of path planning without using the proposed perpendicular path planning method when the narrow passage end is blocked. Due to the minimum cost near the entrance of the passage, the planned path cannot adjust the heading of the AUV to observe the passage. When the AUV entered the passage, it was observed that the front was impassable. Since the space inside the passage is too narrow, it was impossible for the AUV to turn safely, ultimately leading to the collision.

The width of the narrow passage is set to 10 m, and the obstacle parameters are shown in Table 5.

Table 5. Obstacle parameters with impassable narrow passage.

Number	Number of Sides/m	Vertex Coordinates/m
1	4	(910, 700), (910, 1050), (1300, 1050), (1300, 700)
2	3	(900, 1000), (500, 1200), (900, 1300)

The complete path and the number of the sectorial grids selected by the AUV during sailing are illustrated in Figure 14. In this test, the narrow passage is impractical to traverse, and the AUV switched to select the optimal heading of the sectorial grid to detour. The total path length is 1407.1 m, with a total sailing time of 700 s. The obstacle avoidance scenes together with the cost of the sectorial grids at key path points are shown in Figures 15–17.

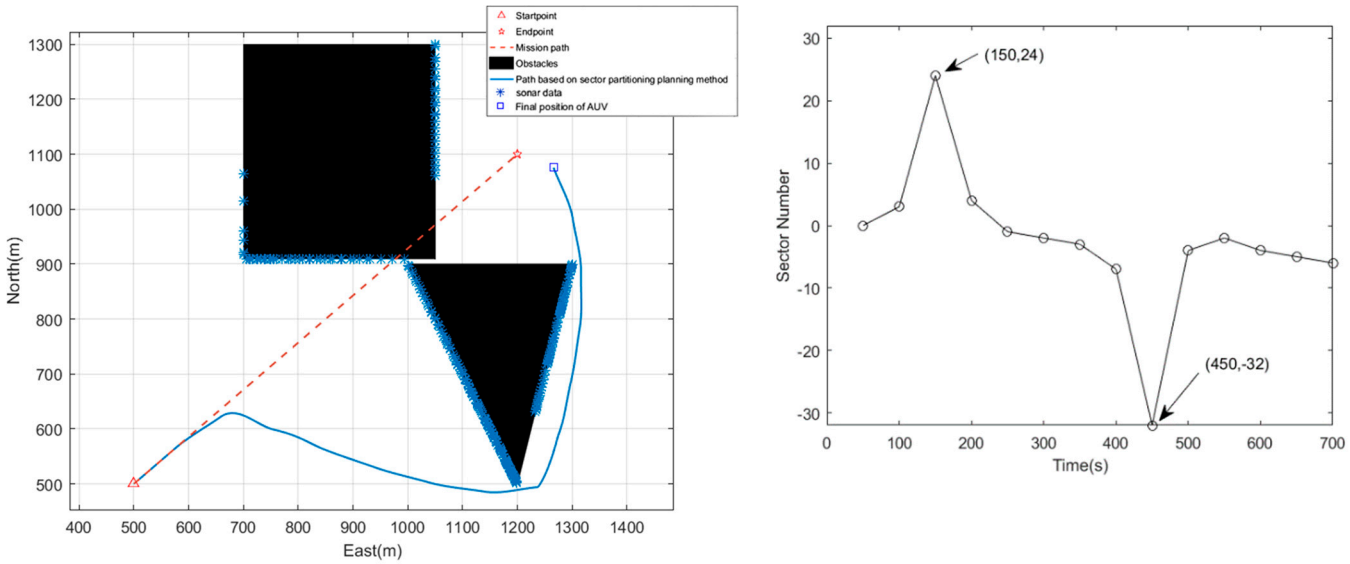

(**a**) (**b**)

Figure 14. Path planning results and fan-shaped grid selection when the width of the narrow passage is too small to pass through. (**a**) Result of detour in the narrow passage scene. (**b**) Sectorial grid selection of the AUV during sailing.

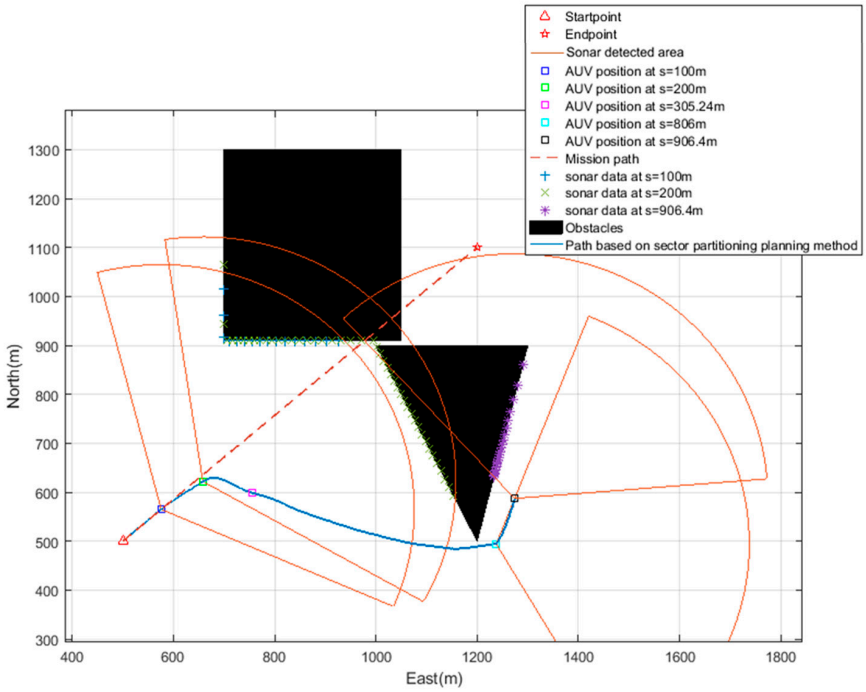

Figure 15. Obstacle avoidance scenarios for the AUV in different positions.

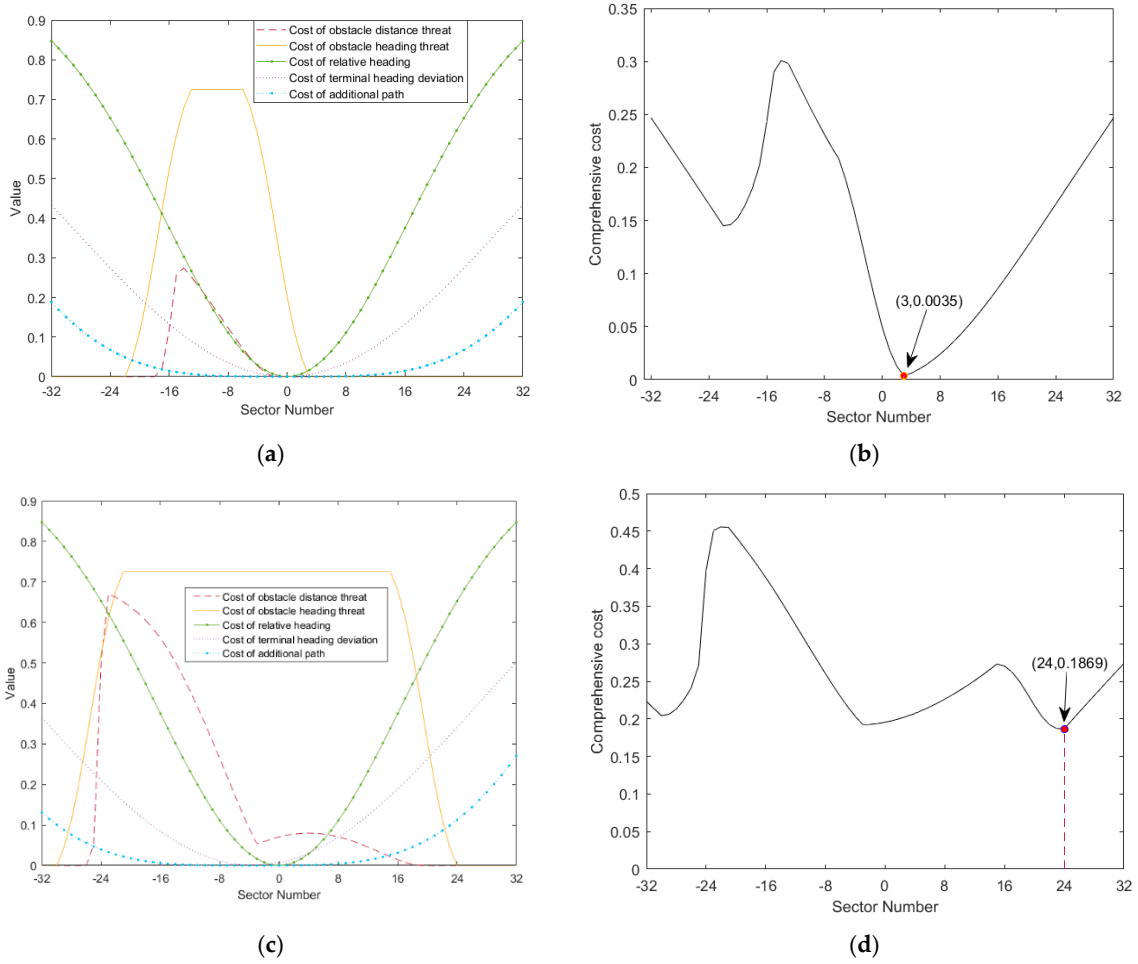

Figure 16. *Cont.*

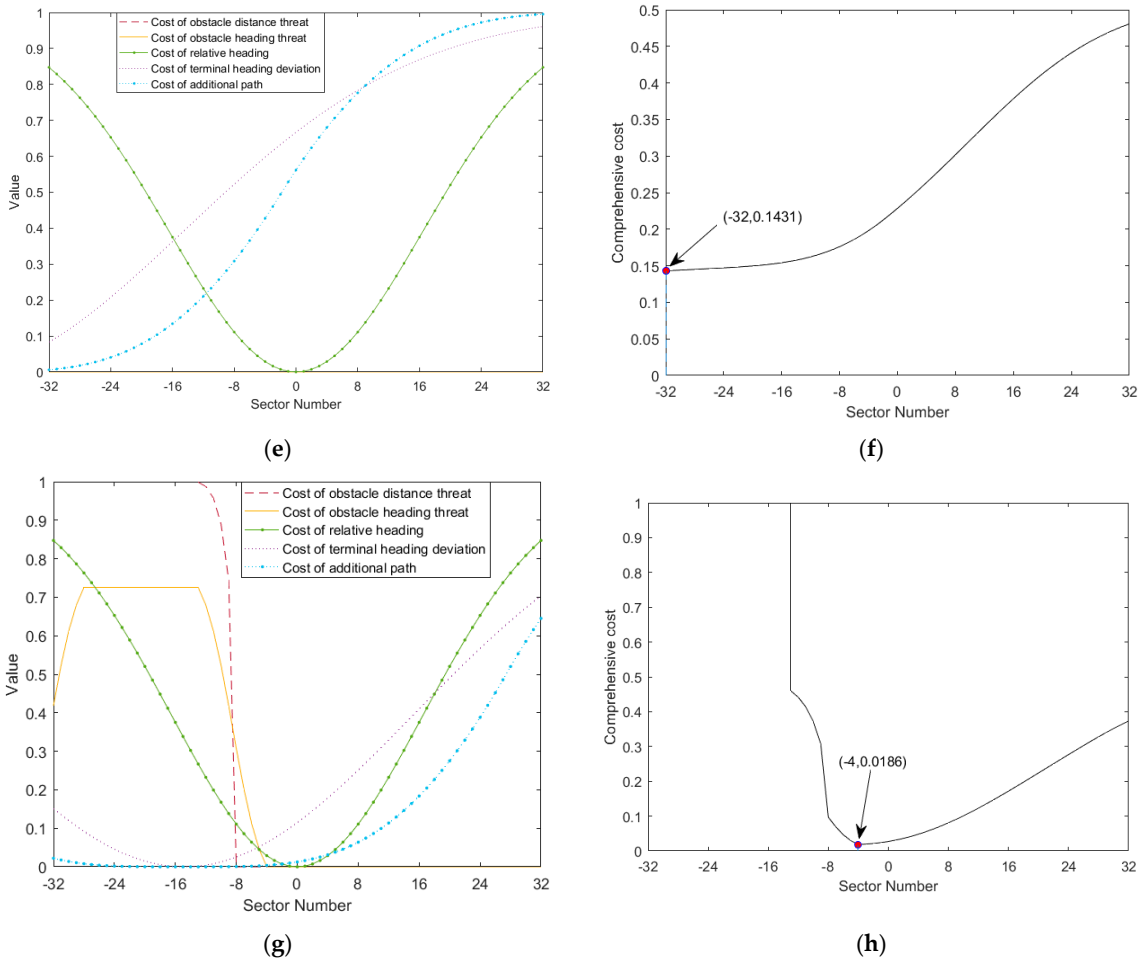

Figure 16. Fan-shaped grid cost for AUVs in different positions. (**a**) Various costs at s = 100 m. (**b**) Comprehensive cost at s = 100 m. (**c**) Various costs at s = 200 m (t = 150 s). (**d**) Comprehensive cost at s = 200 m (t = 150 s). (**e**) Various costs at s = 806 m (t = 450 s). (**f**) Comprehensive cost at s = 806 m (t = 450 s). (**g**) Various costs at s = 906.4 m. (**h**) Comprehensive cost at s = 906.m.

As shown in Figure 14b, the vehicle made sharp turns at 150 s and 450 s, and the corresponding obstacle avoidance scenes and sectorial grid cost during sailing correspond to Figures 15 and 16, respectively. When t = 150 s, threatened by obstacles, the AUV chose sectorial grid 24 for sailing. When t = 450 s, with no obstacle in the sonar detection range, the AUV chose sectorial grid -32 under the constraint of the ending point heading.

After bypassing the obstacles, the AUV navigates towards the target point based on the obstacle avoidance scenario and fan-shaped grid cost shown in Figure 17.

In addition, the coordinates of the ending point in the geodetic coordinate system are set to $(1200, 1200)$, and the complete path planned is shown in Figure 18.

When the AUV was located at $(570.71, 1570.71)$ (s = 100 m), the sonar failed to detect obstacle 2. Affected by the heading threat of obstacle 1, the AUV turned right to avoid it. As the AUV approached the obstacles, when the AUV was located at $(654.58, 625.17)$, threatened by the obstacles, the AUV entailed a big turn to avoid from the side. Constrained by the heading direction of the ending point, the AUV ultimately chose to detour from the left.

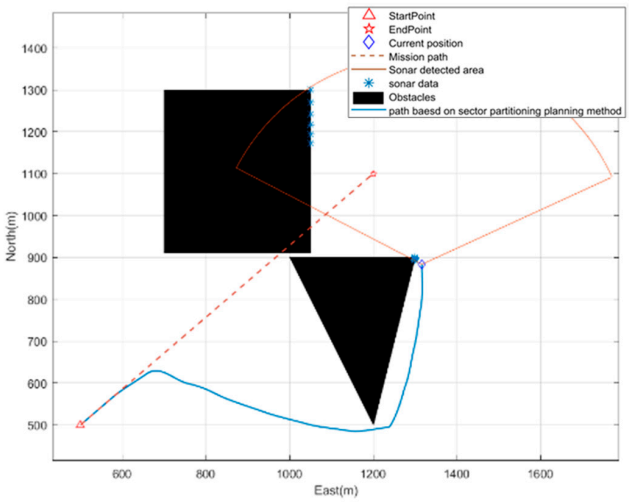

(**a**)

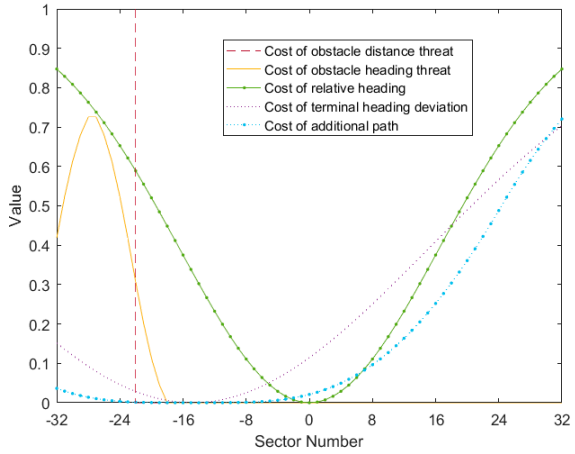

(**b**)

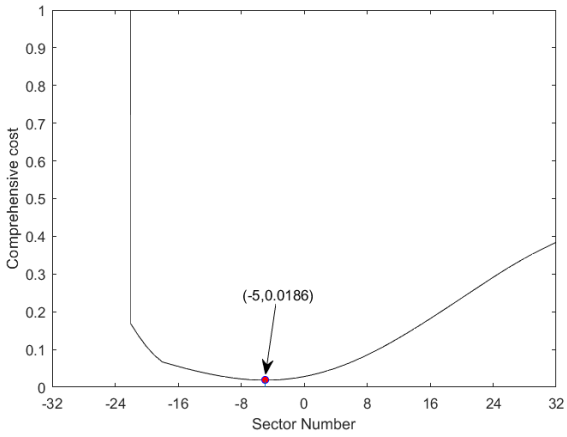

(**c**)

Figure 17. Obstacle avoidance scene and fan-shaped grid cost at s = 1206.7 m. (**a**) Obstacle avoidance scene at s = 1206.7 m. (**b**) Various costs at s = 1206.7 m. (**c**) Comprehensive cost at s = 1206.7 m.

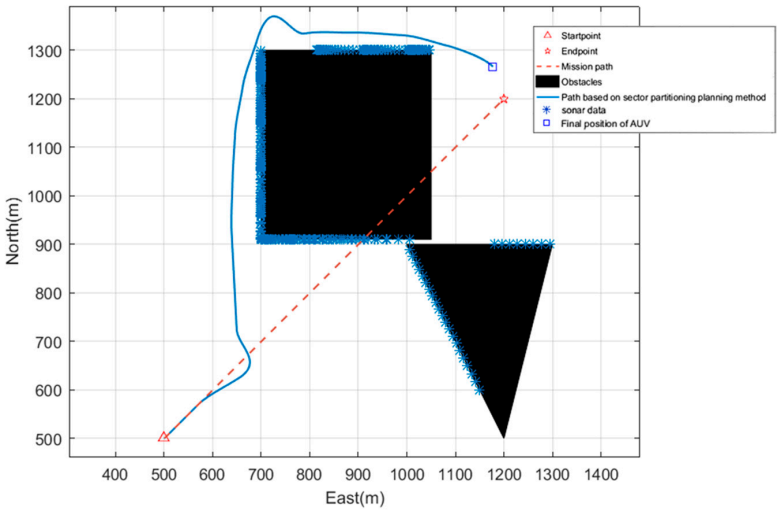

Figure 18. Obstacle avoidance scene with ending point coordinates of (1200, 1200).

5.3. Comparison with VFH Method

To further validate the effectiveness of the proposed algorithm, this study conducts a simulation comparison with the vector field histogram (VFH) method [41]. The experiments are conducted in the environment described in Table 4, where the starting point is located at (500, 500), represented by a red triangle, and the ending point is at (1200, 1200), represented by a red pentagram. The final path nodes of the proposed method and the VFH method for the AUV are represented by blue squares and purple diamonds, respectively, with the final path illustrated in Figure 19. The parameter settings for the VFH method are detailed in Table 6.

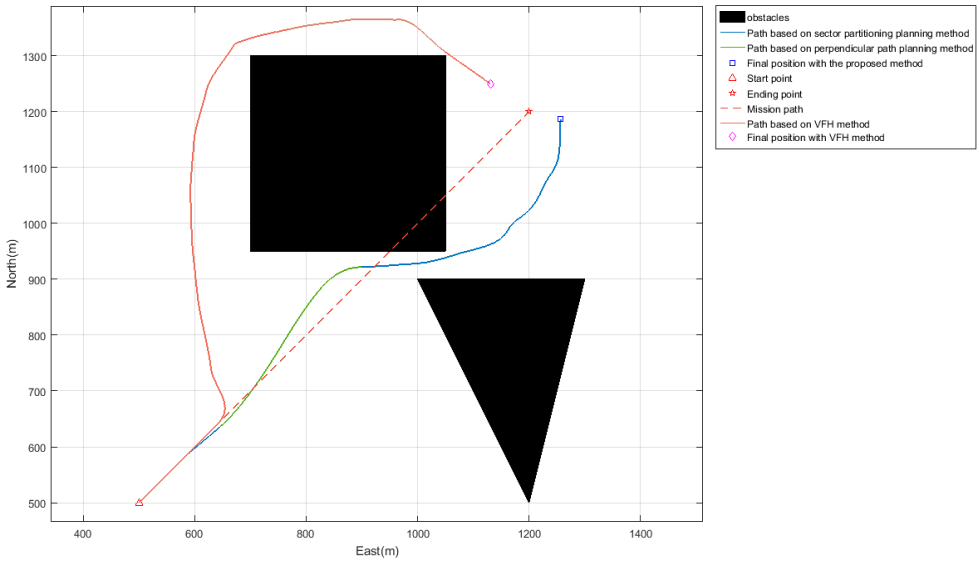

Figure 19. Comparison of path planning results between the proposed method and the VFH method.

Table 6. Parameters in VFH method.

Parameters	Values
Angular resolution f	2°
Wide valley $s_{\max}$	18
Narrow valley $s_{\min}$	4
a	2001
b	2.5
Control Value CV	1.5
Threshold thr	1689.8

Due to the excessively narrow passage between the obstacles, which do not meet the criteria for being considered a narrow valley (the histogram is illustrated in Figure 20), the AUV detoured to the left. The comparison reveals that the proposed method has an advantage in selecting the optimal path, as it takes into account the narrow passage between obstacles. However, it is undeniable that the VFH method is simpler and more user-friendly in practical applications.

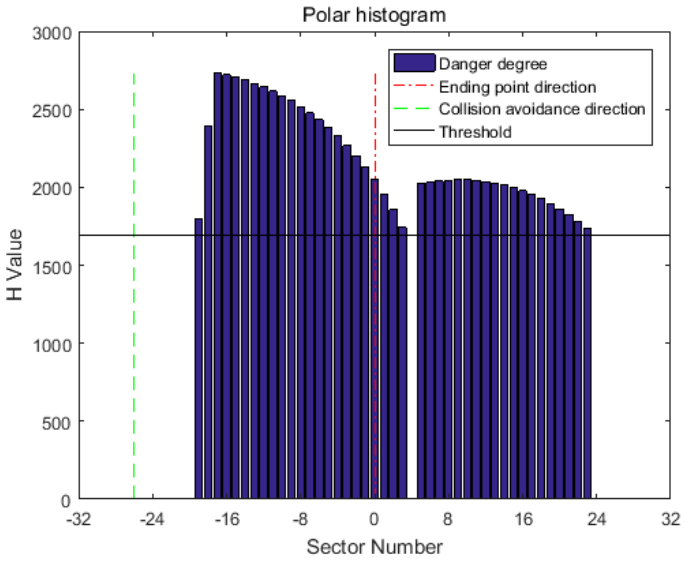

Figure 20. Polar obstacle density in polar histogram.

6. Conclusions

An online path planning method based on a sectorial gridded detection area is proposed. To have a higher efficiency of decision-making, a novel fan-shaped grid environmental model consistent with the actual detection characteristics of sonar is developed. On this basis, the optimal heading for multiple objectives, including safety, smoothness, and cost, can be determined through a heuristic comprehensive cost function in a sectorial grid. Furthermore, a narrow passage traversing strategy using polynomial trajectory planning is proposed by utilizing the perpendicular bisector to locate a series of subgoals. This strategy provides a new solution for the AUV to recognize and safely traverse narrow passages, and it enables early observation of the environment and ensures the AUV sails as closely to the center of the narrow passage as possible. The simulation results indicate that the proposed method enables AUVs to sail with an optimal heading in unknown environments, and the narrow passage traversing strategy can implement collision-free crossing. If the narrow passage is infeasible, the optimal detour direction is determined based on the sectorial grid cost. The proposed method is simple and exhibits real-time performance. It will reduce the probability of wasting feasible threading path that is superior to the detour path.

Author Contributions: Conceptualization, Y.L. and J.S.; methodology, Y.L. and J.S.; software, J.S.; validation, J.S.; formal analysis, G.L.; investigation, X.X.; writing—original draft preparation, J.S.; writing—review and editing, Y.L. and G.L.; project administration, Y.L. and X.X.; funding acquisition, X.X. All authors have read and agreed to the published version of the manuscript.

Funding: Research fund from National Key Laboratory of Autonomous Marine Vehicle Technology (Grant No. 2023-SXJQR-SYSJJ04), National Key Laboratory of Underwater Acoustic Countermeasures (Grant No. CX-2024-011), Natural Science Foundation of Heilongjiang Province (Grant No. LH2023F025), Natural Science Foundation of Shandong Province (Grant No. ZR2022QE056).

Institutional Review Board Statement: Not applicable.

Informed Consent Statement: Not applicable.

Data Availability Statement: The data can be obtained by contacting the corresponding author.

Conflicts of Interest: The authors declare no conflicts of interest.

References

1. Baylog, J.G.; Wettergren, T.A. Online Determination of the Potential Benefit of Path Adaptation in Undersea Search. *IEEE J. Ocean. Eng.* **2014**, *39*, 1165–1178. [CrossRef]
2. Nichols, J.; Woodroffe, A.; Jackson, E.; Johnson, A.; Morgan, M. Subsea Environmental Acoustic Monitoring Using Long Range Autonomous Underwater Vehicles. In Proceedings of the OCEANS Hampton Roads Conference, Hampton Roads, VA, USA, 17–20 October 2022.
3. Wu, H.; He, S.; Deng, Z.; Kou, L.; Huang, K.; Suo, F. Fishery monitoring system with AUV based on YOLO and SGBM. In Proceedings of the 2019 Chinese Control Conference (CCC), Guangzhou, China, 27–30 July 2019.
4. Shi, J.; Zhou, M. A Data-Driven Intermittent Online Coverage Path Planning Method for AUV-Based Bathymetric Mapping. *Appl. Sci.* **2020**, *10*, 6688. [CrossRef]
5. Zhou, M.; Shi, J.; Zhao, L. Towards the Development of an Online Coverage Path Planner for UUV-based Seafloor Survey using an Interferometric Sonar. In Proceedings of the IEEE/OES Autonomous Underwater Vehicles Symposium (AUV), St. Johns, NL, Canada, 30 November–2 October 2020.
6. Li, D.; Wang, P.; Du, L. Path Planning Technologies for Autonomous Underwater Vehicles-A Review. *IEEE Access* **2019**, *7*, 9745–9768. [CrossRef]
7. Li, J.; Zhang, G.; Jiang, C.; Zhang, W. A survey of maritime unmanned search system: Theory, applications and future directions. *Ocean Eng.* **2023**, *285*, 115359. [CrossRef]
8. Hwang, J.; Bose, N.; Fan, S. AUV Adaptive Sampling Methods: A Review. *Appl. Sci.* **2019**, *9*, 3145. [CrossRef]
9. Sheng, L.; Qiu, Z.; Li, H. A Survey on Route Planning Methods of AUV Considering Influence of Ocean Current. In Proceedings of the IEEE 4th International Conference on Control Science and Systems Engineering (ICCSSE), Wuhan, China, 21–23 August 2018.
10. Zhang, H.; Gong, L.; Chen, T.; Wang, L.; Zhang, X. Global Path Planning Methods of UUV in Coastal Environment. In Proceedings of the IEEE International Conference on Mechatronics and Automation, Harbin, China, 7–10 August 2016.
11. Guo, J.; Liu, J.; Liu, M.; Zhang, T.; Yang, T.; Cui, J. Analysis of the Factors Affecting the Communication Between AUV and Acoustic Modem: From the Perspective of Experiments. In Proceedings of the 15th ACM International Conference on Underwater Networks & Systems, Shenzhen, China, 23–26 November 2021.
12. Lin, C.; Wang, H.; Yuan, J.; Yu, D.; Li, C. Research on UUV Obstacle Avoiding Method Based on Recurrent Neural Networks. *Complexity* **2019**, *2019*, 6320186. [CrossRef]
13. Panda, M.; Das, B.; Subudhi, B.; Pati, B.B. A Comprehensive Review of Path Planning Algorithms for Autonomous Underwater Vehicles. *Int. J. Autom. Comput.* **2020**, *17*, 321–352. [CrossRef]
14. Guo, Y.; Liu, H.; Fan, X.; Lyu, W. Research Progress of Path Planning Methods for Autonomous Underwater Vehicle. *Math. Probl. Eng.* **2021**, *2021*, 8847863. [CrossRef]
15. Cheng, C.; Sha, Q.; He, B.; Li, G. Path planning and obstacle avoidance for AUV: A review. *Ocean Eng.* **2021**, *235*, 109355. [CrossRef]
16. Yao, T.; He, T.; Zhao, W.M.; Sani, A.Y. Review of Path Planning for Autonomous Underwater Vehicles. In Proceedings of the International Conference on Robotics, Intelligent Control and Artificial Intelligence (RICAI), Shanghai, China, 20–22 September 2019.
17. Zeng, D.; Chen, S.; Li, Z.; Ma, X.; Xu, Y. Real-time Path Planning for Autonomous Underwater Vehicle Mobile Docking. In Proceedings of the Global OCEANS Singapore—U.S. Gulf Coast Conference, Biloxi, MS, USA, 5–30 October 2020.
18. Dechter, R.; Pearl, J. Generalized Best-First Search Strategies and the Optimality of A*. *J. ACM* **1985**, *32*, 505–536. [CrossRef]
19. Stentz, A. Optimal and efficient path planning for partially-known environments. In Proceedings of the 1994 IEEE International Conference on Robotics and Automation, San Diego, CA, USA, 8–13 May 1994.
20. Khatib, O. Real-time obstacle avoidance for manipulators and mobile robots. In Proceedings of the 1985 IEEE International Conference on Robotics and Automation, St. Louis, MO, USA, 25–28 March 1985.
21. Li, K.; Hu, Q.; Liu, J. Path Planning of Mobile Robot Based on Improved Multiobjective Genetic Algorithm. *Wirel. Commun. Mob. Comput.* **2021**, *2021*, 8836615. [CrossRef]
22. Yu, Z.; Liu, Q.; Zhou, D.; Zhang, Q. Safe and Efficient Mobile Robot Path Planning in Open World Environments. In Proceedings of the International Conference on Mechanical, Automation and Electrical Engineering (CMAEE), Chengdu, China, 16–18 December 2022.
23. Nie, Y.; Yang, H.; Gao, Q.; Qu, T.; Fan, C.; Song, D. Research on Path Planning Algorithm Based on Dimensionality Reduction Method and Improved RRT. In Proceedings of the Global OCEANS Singapore—U.S. Gulf Coast Conference, Biloxi, MS, USA, 5–30 October 2020.
24. Zhang, W.; Wang, N.; Wu, W. A hybrid path planning algorithm considering AUV dynamic constraints based on improved A* algorithm and APF algorithm. *Ocean Eng.* **2023**, *285*, 115333. [CrossRef]
25. Taheri, E.; Ferdowsi, M.H.; Danesh, M. Closed-loop randomized kinodynamic path planning for an autonomous underwater vehicle. *Appl. Ocean Res.* **2019**, *83*, 48–64. [CrossRef]
26. Okereke, C.E.; Mohamad, M.M.; Wahab, N.H.A.; Elijah, O.; Al-Nahari, A.; Zaleha, S.H. An Overview of Machine Learning Techniques in Local Path Planning for Autonomous Underwater Vehicles. *IEEE Access* **2023**, *11*, 24894–24907. [CrossRef]

27. Grefenstette, J.J. Genetic Algorithms for Changing Environments. In Proceedings of the Parallel Problem Solving from Nature 2, Brussels, Belgium, 28–30 September 1992.
28. Colorni, A.; Dorigo, M.; Maniezzo, V.; Varela, F.; Bourgine, P. Distributed optimization by ant colonies. In Proceedings of the First European Conference on Artificial Life, Paris, France, 11–13 December 1991.
29. Kennedy, J.; Eberhart, R. Particle swarm optimization. In Proceedings of the ICNN'95—International Conference on Neural Networks, Perth, WA, Australia, 27 November–1 December 1995.
30. Hadi, B.; Khosravi, A.; Sarhadi, P. Deep reinforcement learning for adaptive path planning and control of an autonomous underwater vehicle. *Appl. Ocean Res.* **2022**, *129*, 103326. [CrossRef]
31. Cao, X.; Chen, L.; Guo, L.; Han, W. AUV Global Security Path Planning Based on a Potential Field Bio-Inspired Neural Network in Underwater Environment. *Intell. Autom. Soft Comput.* **2021**, *27*, 391–407. [CrossRef]
32. Meng, R.; Sun, A.; Wu, Z.; Du, X.; Meng, Y. 3D smooth path planning of AUV based on improved ant colony optimization considering heading switching pressure. *Sci. Rep.* **2023**, *13*, 12348.
33. Yan, Z.; Jiang, L.; Wu, D. A Path Planning Algorithm based on Artificial Potential Field Method and Ant Colony Algorithm. In Proceedings of the 2021 IEEE International Conference on Mechatronics and Automation (ICMA), Takamatsu, Japan, 8–11 August 2021.
34. Xu, J.; Gu, H.; Liang, H. Path Planning for Unmanned Underwater Vehicle Based on Improved Particle Swarm Optimization Method. *Int. J. Online Eng.* **2018**, *14*, 137–149. [CrossRef]
35. Sun, B.; Ma, H.; Zhu, D. A Fusion Designed Improved Elastic Potential Field Method in AUV Underwater Target Interception. *IEEE J. Ocean. Eng.* **2023**, *48*, 640–648. [CrossRef]
36. Yang, L.; Qi, J.; Xiao, J.; Yong, X. A Literature Review of UAV 3D Path Planning. In Proceedings of the 11th World Congress on Intelligent Control and Automation, Shenyang, China, 29 June–4 July 2014.
37. Zhao, J.; Jia, Z.; Zhou, Y.; Zhang, R.; Xie, Z.; Xu, Z. Path Planning based on Multi-objective Topological Map. In Proceedings of the 2021 IEEE Congress on Evolutionary Computation (CEC), Kraków, Poland, 28 June–1 July 2021.
38. Wheare, J.; Lammas, A.; Sammut, K. Toward the Generation of Mission Plans for Operation of Autonomous Marine Vehicles in Confined Areas. *IEEE J. Ocean. Eng.* **2019**, *44*, 320–330. [CrossRef]
39. Zhang, X.; Wang, H.; Lv, H.; Li, Q. UUV Dynamic Path Planning and Trap Escape Strategies in Unknown Environment. In Proceedings of the 35th Chinese Control Conference (CCC), Chengdu, China, 27–29 July 2016.
40. Benjamin, M.R.; Defilippo, M.; Robinette, P.; Novitzky, M. Obstacle Avoidance Using Multiobjective Optimization and a Dynamic Obstacle Manager. *IEEE J. Ocean. Eng.* **2019**, *44*, 331–342. [CrossRef]
41. Borenstein, J.; Koren, Y. The vector field histogram-fast obstacle avoidance for mobile robots. *IEEE Trans. Robot. Automat.* **1991**, *7*, 278–288. [CrossRef]